J Solid State Electrochem (2008) 12:1645–1652
DOI 10.1007/s10008-008-0543-1

ORIGINAL PAPER

High-voltage aqueous symmetric electrochemical capacitor based on $Ru_{0.7}Sn_{0.3}O_2{\cdot}nH_2O$ electrodes in 1 M KOH

Chang-zhou Yuan · Hui Dou · Bo Gao · Ling-hao Su · Xiao-gang Zhang

Received: 24 December 2007 / Accepted: 5 March 2008 / Published online: 9 April 2008

Abstract A mild hydrothermal process is applied to synthesize hydrous ruthenium–tin binary oxides ($Ru_{0.7}Sn_{0.3}O_2{\cdot}nH_2O$) with good capacitive performance in alkaline system. Then, a symmetric electrochemical capacitor (EC) is fabricated based on the as-synthesized $Ru_{0.7}Sn_{0.3}O_2{\cdot}nH_2O$ material and 1 M KOH aqueous electrolyte. Electrochemical performance of the symmetric EC is investigated by cyclic voltammetry, galvanostatic charge–discharge and electrochemical impedance spectroscopy tests. Electrochemical tests demonstrate that the symmetric EC surprisingly can operate with a high upper cell voltage limit of 1.45 V in 1 M KOH electrolyte. Maximum specific capacitance and energy density of the symmetric aqueous EC are approximately 160 F/g and 21 Wh/kg, respectively, delivered at a current density of 1.25 A/g. And the specific energy density decreases to approximately 15 Wh/kg when the specific power density increases up to approximately 1,770 W/kg. The promising specific energy and power densities are obtained simultaneously for the unwonted symmetric EC due to its larger operating potential range. Moreover, the symmetric EC exhibits electrochemical stability with 85.2% of the initial capacitance over consecutive 1,000 cycle numbers.

Keywords $Ru_{0.7}Sn_{0.3}O_2{\cdot}nH_2O$ · Aqueous symmetric electrochemical capacitors · High voltage · Energy density · Power density

C.-z. Yuan · H. Dou · B. Gao · L.-h. Su · X.-g. Zhang (✉)
College of Material Science and Engineering,
Nanjing University of Aeronautics and Astronautics,
Nanjing 210016, People's Republic of China
e-mail: azhangxg@163.com

Abbreviations

ECs	electrochemical capacitors
EIS	electrochemical impedance spectroscopy
CV	cyclic voltammetry
SC	specific capacitance
SED	specific energy density
SPD	specific power density
ECPs	electrical conducting polymers
PANI	polyaniline
Ppy	polypyrrole
PEDOT	poly(3,4-ethy-lenedioxythiophene)
RT	room temperature
AB	acetylene black
PTFE	polytetrafluoroethylene
EDAX	energy-dispersive analysis by X-ray
HRTEM	high-resolution transmission electron microscope

Introduction

Recently, research on the electrochemical capacitors (ECs) has drawn a great deal of attention for use in high-power energy storage devices, due to their many advantages (high power density, long cycle life, etc.) over the second battery and conventional capacitors [1]. However, one key drawback inhibiting the commercialization of ECs, compared to secondary battery, is their lower energy density. Therefore, it would be much better for practical application if an EC with good power property could still deliver higher energy density. It has been well established that the performance of an EC, in terms of energy density, is governed mainly by the specific capacitance (SC) of the electrode materials and the cell working voltage [1]. So, the next logical and feasible procedure to improve the energy

density performance of an EC is to optimize both the SC and the cell potential limit. The former procedure is an intrinsic property of an electrode material but it can be controlled by the improvement of synthetic procedures that synthesize nanostructured material with high effective specific surface area. On the other hand, in particular, the cell voltage is another critical and significant parameter considering that it shows a square dependence with the energy density and that it can be severely limited by the decomposition of water when aqueous electrolyte are used. Therefore, it is imperative and urgent to circumvent the narrow electrochemical window for aqueous symmetric ECs.

Unfortunately, these requirements (high SC and large cell voltage) are difficult to fulfill simultaneously for an aqueous symmetric EC. Aqueous supercapacitors based on RuO_2 with high single-electrode SC are just performed within the working voltage window of 0.8 V in 1 M KOH aqueous electrolyte [2, 3]. The cell voltages of MnO_2–MnO_2 and Fe_3O_4–Fe_3O_4 symmetric ECs are just 1.0 and 0.6 V, respectively, in aqueous K_2SO_4 medium [4]; The NiO–NiO and porous Ni–porous Ni symmetric devices both only work within a 1.0-V potential window in 6 M KOH aqueous solution [5]. Symmetric cells based on electrical conducting polymers, such as polyaniline, polypyrrole, and poly(3,4-ethy-lenedioxythiophene), can just operate in cell voltage of less than 0.7 V [6]. In addition, for symmetric ECs based on carbon materials, their electrochemical windows have not gone beyond the 1.0 V limit yet in 1 M H_2SO_4 [6]. To obtain even larger working voltage for symmetric ECs, commonly, it can be achieved only with carbon materials [7] combined with hazardous organic solvents [8] or solvent-free ionic liquid [9]. However, from the application point of view, it is ideal and desirable that the novel aqueous devices with high cell voltage limit, based on certain unique electroactive materials, can increase the energy density significantly and at the same time maintain the extended cycle life and the fast charge–discharge capability of the device.

Hydrous ruthenium–tin binary oxides have been found to exhibit good electrochemical capacitive performance and extensively investigated in H_2SO_4 medium with three-electrode system [10–13]. The introduction of SnO_2 is believed to not only increase the utilization of Ru species but also enhance the electrochemical stability although pseudocapacitance of the binary oxides should be mainly contributed by the electroactive oxyruthenium species (i.e., RuO_2) [10–13]. However, the capacitive performance of the binary oxide, to the best of our knowledge, has not been investigated in an alkaline system. Moreover, alkaline KOH aqueous solution has also been shown as another good electrolyte for Ru-based oxide electrodes [14–18].

Herein, $Ru_{0.7}Sn_{0.3}O_2\ nH_2O$ has been prepared by means of mild hydrothermal process and its electrochemical performance also has been investigated in 1 M KOH aqueous medium. Then, an aqueous symmetric EC based on the as-synthesized $Ru_{0.7}Sn_{0.3}O_2\ nH_2O$ electrodes has been first assembled with 1 M KOH aqueous solution. Electrochemical tests demonstrate that the aqueous symmetric EC owns good electrochemical performance in such alkaline system. Unexpectedly, an impressive working cell voltage limit of 1.45 V in 1 M KOH electrolyte is first realized for the unwonted aqueous symmetric EC based on the electroactive material $Ru_{0.7}Sn_{0.3}O_2\ nH_2O$.

Experimental

Synthesis and characterization of $Ru_{0.7}Sn_{0.3}O_2{\cdot}nH_2O$

The method employed for the synthesis of $Ru_{0.7}Sn_{0.3}O_2{\cdot}nH_2O$ was by means of mild hydrothermal route as described in [10], except where otherwise specified. $RuCl_3$ and $SnCl_4$ solutions (the molar ratio of Ru^{3+} and Sn^{4+} was 7: 3) were agitated at room temperature (RT) for 30 min and then ultrasonically treated for 10 min. After being well mixed, the precursor solution, whose total concentration was 20 mM, was kept in a Teflon-lined autoclave with a stainless steel shell. After being heated to 180 °C, the autoclave was kept at the temperature for 5 h in an oven and then cooled to RT naturally. The product of the reaction was filtered, washed repeatedly with distilled water and ethanol, and then dried at 80 °C. For comparison, $RuO_2{\cdot}nH_2O$ was also synthesized as the described method above just with the exception of the addition of Sn species into the precursor solution. The morphologies of the sample were examined by high-resolution transmission electron microscope (HRTEM; Hitachi-600, Japan). The X-ray diffraction (XRD) pattern of the sample was observed by XRD (Max 18 ^{XCE}, Japan) using a Cu Ka source and energy-dispersive analysis by X-ray (EDAX, Link-200, Britain).

Electrochemical tests

Electrodes were prepared by mixed 5 mg $Ru_{0.7}Sn_{0.3}O_2{\cdot}nH_2O$, acetylene black (AB) with the mass ranged from 0.5 to 1.75 mg and polytetrafluoroethylene (PTFE) with the mass ranged from 0.5 to 2 mg. The mixture was thoroughly ground in a mortar and then three drops of 1-M KOH solution was then added to this composite to form a more homogeneous slurry, which was pressed (1.2×10^7 Pa) onto nickel grid (1 cm^2) serving as a current collector and dried at 100 °C. The typical loading of electroactive material $Ru_{0.7}Sn_{0.3}O_2{\cdot}nH_2O$ was 5 mg. The thickness of the

electrodes was ranged from approximately 350 to 440 μm. Electrochemical measurement of as-prepared $Ru_{0.7}Sn_{0.3}O_2{\cdot}nH_2O$ in 1 M KOH aqueous electrolyte was made on a three-electrode cell equipped with a working electrode, a platinum plate counter electrode, and an Hg–HgO reference electrode. And the optimization of the electrode composition was made based on the same mass of the electroactive material $Ru_{0.7}Sn_{0.3}O_2{\cdot}nH_2O$ and the changing masses of the AB and PTFE, respectively.

Electrodes for the symmetric ECs were all prepared by mixed 5 mg $Ru_{0.7}Sn_{0.3}O_2{\cdot}nH_2O$ ($RuO_2{\cdot}nH_2O$) with 1.5 mg AB and 0.5 mg PTFE. All the electrochemical measurements for the symmetric device were performed in two-electrode cell configures assembled with two face-to-face $Ru_{0.7}Sn_{0.3}O_2{\cdot}nH_2O$ (or $RuO_2{\cdot}nH_2O$) electrodes immerged and separated by a distance of approximately 1 cm in 1-M KOH aqueous solution in a glass vial. The cell was not thermostated; however, the ambient temperature was between 20 and 25 °C. Electrochemical performance was evaluated by cyclic voltammetry (CV) performed on CHI660 electrochemical workstation system, galvanostatic charge–discharge tests carried out with a BT2042 battery tester in a certain range of potentials, and electrochemical impedance spectroscopy (EIS) measured with a frequency response analyzer (Solatron 1255 B) interfaced with a potential galvanostat (Solatron 1287) controlled by a personal computer. The sinusoidal excitation voltage applied to the cell was 5 mV with a frequency range of between 10^5 and 10^{-2} Hz.

Results and discussion

The characteristics of $Ru_{0.7}Sn_{0.3}O_2{\cdot}nH_2O$

The typical XRD pattern of $Ru_{0.7}Sn_{0.3}O_2{\cdot}nH_2O$ is shown in Fig. 1a. All these diffraction peaks of the as-synthesized $Ru_{0.7}Sn_{0.3}O_2{\cdot}nH_2O$, not only the peak position but also their relative intensities, are in good agreement with those recently reported in [10]. In addition, due to the absence of peaks for pure RuO_2 and SnO_2 among these diffraction peaks, the $Ru_{0.7}Sn_{0.3}O_2{\cdot}nH_2O$ should be a solid solution rather than the simple mixture of RuO_2 and SnO_2, which has been verified in [10]. From EDAX data (the inset in Fig. 1a), the existence of Ru and Sn species can be found. Moreover, the molar ratio of the two species is basically in agreement with that added into the precursor solution, suggesting that most Ru and Sn oxides were completely precipitated, which also has been confirmed by the report [10]. In addition, obvious broad diffraction peaks should result from the formation of hydrous Ru–Sn binary oxide in the nanometer scale, which can be further verified by its HRTEM in Fig. 1b. It is clear, from Fig. 1b, that the particle size of the oxide is relatively uniform and ranged from approximately 2 to 4 nm.

Electrochemical behavior of $Ru_{0.7}Sn_{0.3}O_2{\cdot}nH_2O$

The voltammetric charge integrated from a positive or negative sweep of CV plots can be used as an effective signal in determining the pseudocapacitance in redox transitions. Herein, the composition optimization of the prepared $Ru_{0.7}Sn_{0.3}O_2{\cdot}nH_2O$ electrodes has been first investigated by the CV method in 1-M KOH aqueous solution, due to the great influence [19, 20] of the electrode composition (such as, the content of AB, PTFE) upon the electrochemical performance of the electroactive material $Ru_{0.7}Sn_{0.3}O_2{\cdot}nH_2O$. And the average SCs of the $Ru_{0.7}Sn_{0.3}O_2{\cdot}nH_2O$ electrode can be calculated according to the following Eq. 1:

$$SC = \frac{it}{m\Delta V} = \frac{I}{v} \tag{1}$$

where m is the Ru–Sn binary oxide mass (gram) in an electrode, i the current (ampere); t the time (second); ΔV the potential difference (volt); then $I=i/m$ (ampere per gram, with respect to the mass of electroactive material Ru–Sn binary oxide per electrode) and $v=\Delta V/t$ (millivolt per second).

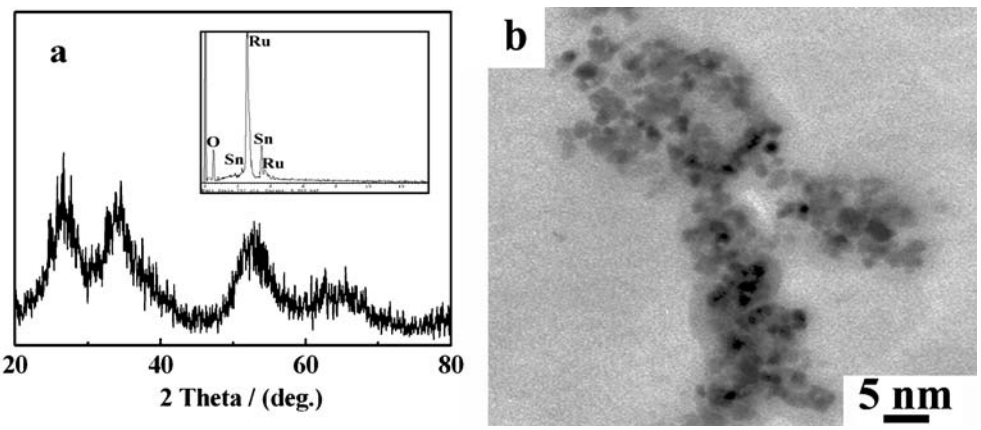

Fig. 1 XRD pattern (**a**), EDAX (the inset in **a**) and HRTEM (**b**) of as-synthesized $Ru_{0.7}Sn_{0.3}O_2{\cdot}nH_2O$

Firstly, on the consumption of the unchanging masses of PTFE and $Ru_{0.7}Sn_{0.3}O_2{\cdot}nH_2O$ in the electrodes, the electrochemical performance of the electrodes are evaluated by changing the mass of AB from 0.5 to 2 mg in the electrodes. The electrochemical data in Fig. 2a demonstrate that the SCs of $Ru_{0.7}Sn_{0.3}O_2{\cdot}nH_2O$ increase greatly with the increase of the mass of AB, the reason for which may be that the more the mass of AB in the electrode is, the better the surface utilization of the Ru–Sn binary oxide and the conductivity of the electrodes are [19, 20]. However, the mass of AB is further enhanced from 1.5 to 1.75 mg; the SC increases very little, which may be related to the increase of the thickness [21] of the electrode due to much more AB in the electrode. Thus, we chose the better weight ratio of $Ru_{0.7}Sn_{0.3}O_2{\cdot}nH_2O$ to AB as 5:1.5. And then based on 5 mg $Ru_{0.7}Sn_{0.3}O_2{\cdot}nH_2O$ and 1.5 mg AB, we further change the mass of PTFE from 0.5 to 2 mg. From the electrochemical data shown in Fig. 2a, evidently, with the increase of the mass of PTFE, the SC of $Ru_{0.7}Sn_{0.3}O_2{\cdot}nH_2O$ decreases greatly, for which the bigger resistance of the electrode should be responsible in the case of higher content of PTFE in the electrode [19, 20]. According to the above discussion, the better electrode composition was chosen as 5 mg $Ru_{0.7}Sn_{0.3}O_2{\cdot}nH_2O$, 1.5 mg AB, and 0.5 mg PTFE, on which the following tests for the electrochemical performance of the symmetric $Ru_{0.7}Sn_{0.3}O_2{\cdot}nH_2O$ EC are all based.

And the typical CV curves (solid lines), from −0.8 to 0.4 V (vs. Hg–HgO), of the $Ru_{0.7}Sn_{0.3}O_2{\cdot}nH_2O$ electrode with the better composition are shown in Fig. 2b at different scan rates as indicated. As seen from Fig. 2b, obviously, the CV curves of the $Ru_{0.7}Sn_{0.3}O_2{\cdot}nH_2O$ are quasirectangular and the electrochemical response currents on the positive sweeps are mirror-image, symmetric to their corresponding counterparts on the negative sweeps. As scan rate increases, the current subsequently increases while the shape of CV curves changes little, which indicates good electrochemical capacitive nature for the binary oxides in 1 M KOH electrolyte. For comparison, the CV curves (dot lines) of $RuO_2{\cdot}nH_2O$ electrode were also demonstrated in Fig. 2b. Clearly, with the introduction of tin species into the ruthenium oxide, the same upper potential limits of 0.4 V are for both ruthenium oxide and Ru–Sn binary oxide electrodes. While the poor rectangular shape for ruthenium oxide electrode is presented in the same potential range as that of Ru–Sn binary oxide electrode. When the potential shifts negatively, the polarization is much clearer for ruthenium oxide electrode in contrast with $Ru_{0.7}Sn_{0.3}O_2{\cdot}nH_2O$ electrode. Therefore, the usable potential range of ruthenium oxide is a little narrower than that of Ru–Sn binary oxide electrode. The reasons for the larger electrochemical window of Ru–Sn binary oxide just after the introduction of Sn species may be ascribed to the improvement of the electrochemical stability of the binary oxide due to the mere doping of Sn species [10–13]. In addition, from the CV curves, the SCs of the $Ru_{0.7}Sn_{0.3}O_2{\cdot}nH_2O$ electrode can be calculated, according to the above Eq. 1, as approximately 434 and 441 F/g, respectively, at the scan rates of 10 and 5 mV/s, respectively.

Electrochemical properties of the aqueous symmetric EC based on $Ru_{0.7}Sn_{0.3}O_2{\cdot}nH_2O$

Typical cyclic voltammograms for the aqueous symmetric EC based on the $Ru_{0.7}Sn_{0.3}O_2{\cdot}nH_2O$ are demonstrated in Fig. 3 at sweep rates of 5, 10, 20, 30, 50 mV/s, respectively. As can be seen from Fig. 3, the CV curves of the $Ru_{0.7}Sn_{0.3}O_2{\cdot}nH_2O$ EC show no peaks, indicating that the EC, in 1 M KOH aqueous medium, is charged and discharged at a pseudoconstant rate over the complete voltammetric cycle, as solution resistance can distort current response at the switching potential, and the distortion is dependent upon the scan rate [22]. At lower scan rate (such as 5, 10, and 20 mV/s), the symmetric EC shows almost ideal capacitive behavior. Although with the scan rate increasing to higher scan rates (such as 30 and 50 mV/s), some deviation from rectangularity of the CV occurs, the CV curves still reveal the good capacitive performance for the symmetric EC. Moreover, it is surprising and impressive that the operating voltage range of the aqueous symmetric EC can be extended up to 1.5 V

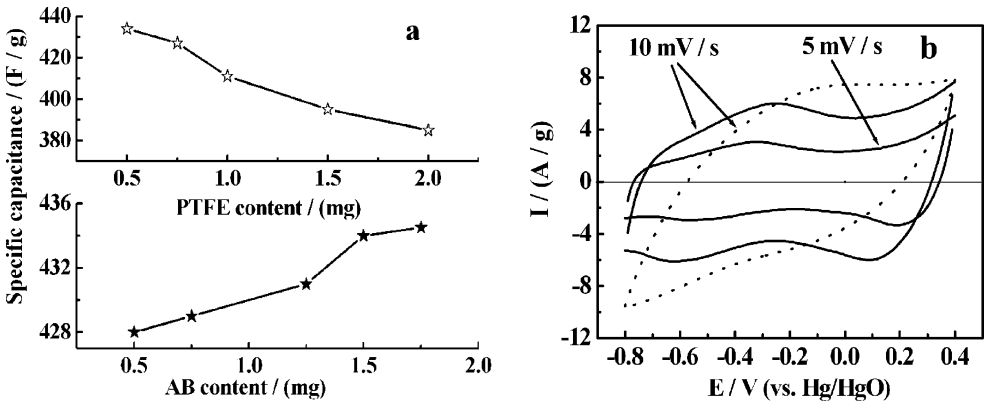

Fig. 2 The influence (**a**) of AB and PTFE on the performance of Ru–Sn binary electrodes; and the CV curves (**b**) at various scan rate for the $Ru_{0.7}Sn_{0.3}O_2{\cdot}nH_2O$ (*solid lines*) electrode with the composition of 5 mg $Ru_{0.7}Sn_{0.3}O_2{\cdot}nH_2O$, 1.5 mg AB, and 0.5 mg PTFE and for the $RuO_2{\cdot}nH_2O$ (*dot lines*) electrode at 10 mV/s

in an aqueous alkaline medium. And for comparison, the CV curves of the symmetric EC based on the $RuO_2{\cdot}nH_2O$ electrode in the same potential range as that of the $Ru_{0.7}Sn_{0.3}O_2{\cdot}nH_2O$ EC are also presented in Fig. 3 (see the inset). When the potential goes beyond 1.0 V, the polarization is obviously presented. Moreover, when the potential starts from 0.8 V, the electrolyte turns out to a red brown color due to the dissolution of Ru species at higher potential, which means that the real working cell potential of the $RuO_2{\cdot}nH_2O$ symmetric EC should not exceed 1.0 V. Therefore, due to the mere introduction of Sn species, the stable electrochemical window of $Ru_{0.7}Sn_{0.3}O_2{\cdot}nH_2O$ EC in alkaline electrolyte is much larger than that of the RuO_2–RuO_2 symmetric system, which is also consistent with the previous reports [2, 3]. Such cell voltage can be comparable to or even lager than some asymmetric systems [23–28]. Although the genuine reasons why the symmetric EC can work beyond 1 V, and even to 1.5 V, in alkaline, aqueous electrolyte are not very clear temporarily; one thing is certain that, out of question, the Sn species plays a very important role in the extension of electrochemical window of the symmetric device because it is just after the introduction of Sn species that the electrochemical window turns out to be much larger on the condition that the other factors are the same. Thereupon, the tentative explanation for such larger operating electrochemical window should be that the introduction of Sn species into the RuO_2 matrix enhances the electrochemical stability of Ru species greatly in the alkaline medium, which have been confirmed by several researchers [29–34].

Also, based on the CV curves in Fig. 3, the SC of 192 F/g for the cell at a sweep rate of 5 mV/s can be obtained according to the above Eq. 1; even at higher sweep rate of 50 mV/s, the SC of 107 F/g still can be delivered for the EC.

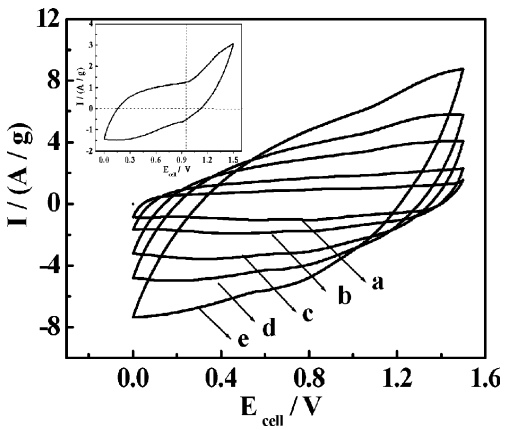

Fig. 3 Cyclic voltammograms for aqueous symmetric EC based on $Ru_{0.7}Sn_{0.3}O_2{\cdot}nH_2O$ at different scan rates: (*a*) 5 mV/s; (*b*) 10 mV/s; (*c*) 20 mV/s; (*d*) 30 mV/s; (*e*) 50 mV/s, respectively, and the inset is the CV curves for aqueous symmetric EC based on $RuO_2{\cdot}nH_2O$ at 10 mV/s

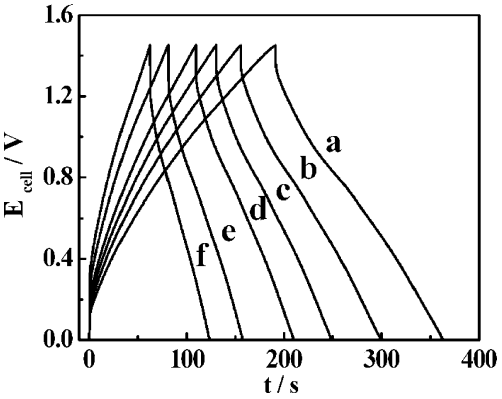

Fig. 4 Galvanostatic charging/discharging curves of the symmetric EC based on $Ru_{0.7}Sn_{0.3}O_2{\cdot}nH_2O$ at different current density: (*a*) 1.25 A/g; (*b*) 1.5 A/g; (*c*) 1.75 A/g; (*d*) 2 A/g; (*e*) 2.5 A/g; (*f*) 3 A/g, respectively

Galvanostatic constant current charge–discharge measurements at different current densities are applied to evaluate the electrochemical properties and to quantify the SC of the symmetric EC in 1 M KOH electrolyte. Figure 4 shows the charge–discharge curves of the symmetric EC at different current densities (current divided by the mass of $Ru_{0.7}Sn_{0.3}O_2{\cdot}nH_2O$ within one electrode) within an electrochemical window from 0.00 to 1.45 V. As seen from Fig. 4, the galvanostatic constant charge–discharge curves behave as symmetric triangular shape during the charge–discharge processes, which resemble those of electrochemical double-layer capacitors. However, a closer look indicates that the slopes of the galvanostatic charge–discharge curves slightly differ from linearity as a result of the pseudo-Faradaic processes for the oxide electrodes. In general, the discharge profile of the symmetric device contains two parts: the resistive component (a sudden voltage drop (IR drop)) representing the voltage change due to the internal resistance of the EC and the capacitive component related to the voltage change due to the change in energy within the symmetric EC. Moreover, IR drop is larger at higher current density because of the domination of a resistive component while at a low current density, due to the domination of a capacitive component, the length of linear portion is larger [29]. The SCs of the symmetric EC at various current densities could be calculated according to Eq. 1 and shown in Table 1. It is noteworthy that such values can be even compared with those of some unsymmetrical devices [23–26].

In addition, the specific energy density (SED) of the symmetric EC can be calculated by means of the following Eq. 2 and the typical results are shown in Table 1.

$$\mathrm{SED} = \frac{1}{4}\mathrm{SC}(\Delta V)^2 \tag{2}$$

Table 1 The SCs and SED of $Ru_{0.7}Sn_{0.3}O_2{\cdot}nH_2O$ symmetric EC based on the curves in Fig. 4

Current density (A/g)	1.25	1.50	1.75	2.00	2.50	3.00
SC (F/g)	160	160	158	157	156	155
SED (Wh/kg)	21	20	19	17	16	15

When the constant current is used for charging and discharging processes, an important parameter, coulombic efficiency (η), can be evaluated from the Eq. (3):

$$\eta = \frac{t_D}{t_C} \times 100\% \tag{3}$$

where t_D and t_C are the time for galvanostatic discharging and charging, respectively.

The power property is one of the main concerns for such an aqueous symmetric EC based on the electroactive material $Ru_{0.7}Sn_{0.3}O_2{\cdot}nH_2O$ in 1 M KOH electrolyte, which can be characterized by the dependence of SCs on the charge–discharge current density (Fig. 5, a). As shown in Fig. 5 (a), the discharge capacitance of the symmetric EC is approximately 160 F/g at a discharge current of 1.25 A/g and then reduces to 155 F/g at a discharge current density of 3 A/g. Also, the SC at a current density of 3 A/g still can be delivered as approximately 97% of that at 1.25 A/g for the cell. Such result suggests that the aqueous symmetric EC has good rate capability, which indicates its possible use in electrochemical devices devious of intermittent high pulse power. In addition, the relationship between charge–discharge current density and coulombic efficiency of the symmetric EC is presented in Fig. 5 (b). From Fig. 5 (b), it is clear that the coulombic efficiencies at different current densities are all more than 92%. Moreover, the coulombic efficiency increases from approximately 92.1% at a current density of 1.25 A/g to approximately 99.5% at a current density of 3 A/g.

In order to further highlight the electrochemical performance of the symmetric device based on $Ru_{0.7}Sn_{0.3}O_2{\cdot}nH_2O$ electrodes, the Ragone plot relating power density to achievable energy density of the symmetric EC at different constant current densities based on the discharge curves is also depicted in Fig. 6. The specific power density (SPD) of the symmetric EC can be calculated from the following equation:

$$\mathrm{SPD} = \frac{I\Delta V}{4} \tag{4}$$

where I and ΔV are the constant charge–discharge current density (ampere per gram, with respect to the mass of electroactive material per electrode) and the potential range (ΔV=1.45 V−IR, where IR is the ohmic drop) of the symmetric EC, respectively. It is evident that the SPD of 1,770 W/kg and SED of approximately 15 Wh/kg are obtained at a current density of 3 A/g. And the SED increases to approximately 21 Wh/kg when the SPD decreases to approximately 850 W/kg. Although these values should be scaled down for a packaged device because the total weight of the device must be considered, such high SED and SPD for the aqueous symmetric EC, out of question, is impressive and contributed by the larger cell voltage range, which is realized in such unwonted symmetric EC. If the SC of $Ru_{0.7}Sn_{0.3}O_2{\cdot}nH_2O$ is further increased greatly, it is not impossible to obtain the much higher specific energy density and power density because the SC of hydrous Ru–Sn binary oxide electrode reported here is even less than those in [10–12].

Impedance spectroscopy is an ideal tool for characterizing ECs because it provides some important information on the time scales of all the phenomena occurring in the device and knowing the parameters involved in each step of the electrochemical process is very useful for the optimization of the ECs [35]. The electrochemical impedance spectrum of the aqueous symmetric EC with 1 M KOH is fitted and shown in Fig. 7.

Based on the statistics in Table 2 and Nyquist plot of the EC in Fig. 7, several features should be described. First, high-frequency intercept of the real axis, the internal resistance (R_s), including the resistance of electrolyte, the

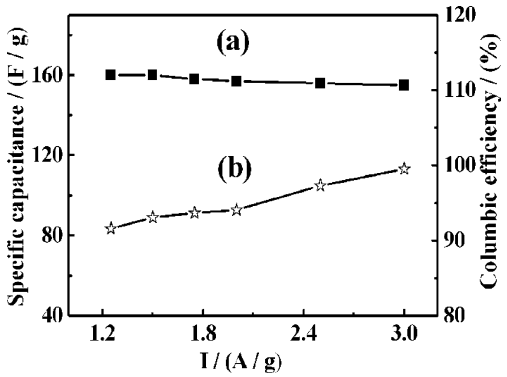

Fig. 5 SCs (*a*) and columbic efficiency (*b*) of symmetric EC based on $Ru_{0.7}Sn_{0.3}O_2{\cdot}nH_2O$ as a function of charge–discharge current density

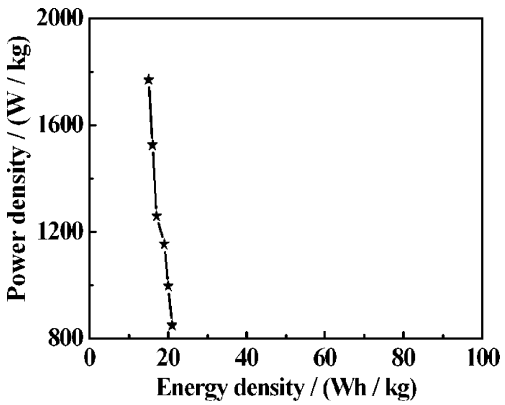

Fig. 6 Ragone plot for symmetric EC based on $Ru_{0.7}Sn_{0.3}O_2{\cdot}nH_2O$ electrodes

intrinsic resistance of active material, and the contact resistance at the interface of active material and current collector, is demonstrated as little as approximately 1.12 Ω for such symmetric EC. Secondly, in high-frequency range, a little semicircle, resulting from the parallel combination of double-layer capacitance (C_{dl}) and charge transfer resistance (R_{CT}) at the compound–electrolyte interface [36, 37], reveals the small R_{CT} and C_{dl}, which are approximately 0.65 Ω and 1.324 F/g, respectively, for the symmetric EC. Thirdly, in the intermediate-frequency region, the 45° line region is clear, suggestive of the existence of finite-length Warburg resistance (Z_W) in the ion diffusion into the porous structure of the electrode. The value for Z_W is approximately 6 Ω. Finally, in the low frequency, the linear region leans more towards imaginary axis and this indicates good capacitive behavior (as the angle φ approaches approximately 90°, it exhibits a good capacitive behavior) for the symmetric device. Also, the SC of the symmetric EC at the open-circuit potential can be evaluated from the EIS test at 0.01 Hz according to the following equation:

$$SC = \frac{1}{mj\omega Z``} \tag{5}$$

where $j=-1$; $\Omega=2\pi f$ (f for the frequency, 0.01 Hz); $Z``$ is the imaginary part of the impendence and m is the mass of the electroactive material in one electrode. An SC of approximately 196.4 F/g can be obtained from the EIS test.

And the corresponding solid line represents the best-fit curve in terms of the fitting equivalent-circuit model (the inset in Fig. 7) for the symmetric EC, where the physical meanings of R_s, R_{ct}, Z_W, and C_{dl} are internal resistance, ionic and electron charge transfer resistance at the electroactive material/electrolyte interface, Warburg diffusion impedance, and double-layer capacitance, respectively. The good fitting indicates that the equivalent-circuit model reasonably represents the electrochemical processes occurring in the symmetric EC. The best-fit values of the equivalent-circuit elements are listed in Table 2.

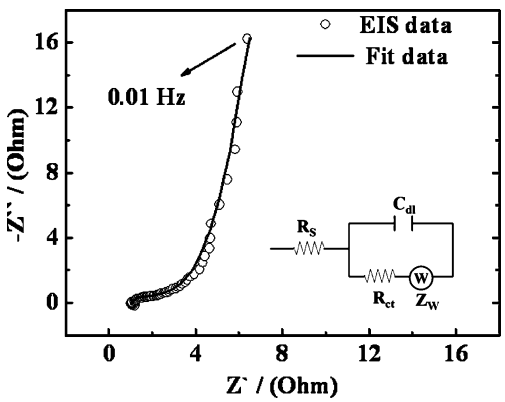

Fig. 7 Nyquist plot of symmetric EC based on $Ru_{0.7}Sn_{0.3}O_2{\cdot}nH_2O$ electrodes

Table 2 The values of the equivalent-circuit elements for the symmetric EC

	R_S (Ω)	C_{dl} (F/g)	R_{CT} (Ω)	Z_W (Ω)
Ru–Sn binary symmetric EC	1.12	1.32	0.65	6.00

The stability of the symmetric EC based on $Ru_{0.7}Sn_{0.3}O_2{\cdot}nH_2O$, during electrochemical cycling for continuous 1,000 cycles without relaxation within the electrochemical window from 0.00 to 1.45 V, is shown in Fig. 8 (the inset is the charge–discharge curves at 1st cycle and 1,000th cycle, respectively, as indicated.). As shown in Fig. 8, the capacitance of the symmetric EC decreases with the growth of the cycle number. Clearly, in the first approximately 300 cycles, the degradation speed of SC is great. And then the SC is relatively stable. After continuous 1,000 cycles, the capacitance value remains approximately 85.2% of that of the first cycle. The attenuation of the capacitance just for 14.8% suggests the certain cyclic stability of the symmetric EC, which is significant for the practical application. Although there is no visible gas evolution occurring during the continuous cycling, the issue of gas still be paid much more attention and will be further detailed in our forthcoming research.

Conclusions

In conclusion, first, $Ru_{0.7}Sn_{0.3}O_2{\cdot}nH_2O$ synthesized via mild hydrothermal method was found to own good electrochemical performance in the voltage from −0.8 to 0.4 V (vs. Hg–HgO). And then, an unwonted aqueous symmetric EC, based on the as-prepared $Ru_{0.7}Sn_{0.3}O_2{\cdot}nH_2O$, with high operating cell voltage of 1.45 V in 1-M KOH electrolyte solution was first proposed. Electrochemical tests revealed that the

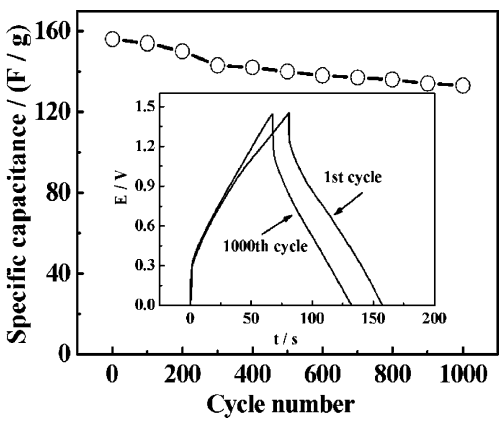

Fig. 8 Cycle-life performance of the $Ru_{0.7}Sn_{0.3}O_2{\cdot}nH_2O$ symmetric EC during multicycles at constant current density of 2.5 A/g between 0.0 and 1.45 V

aqueous symmetric EC owned good electrochemical performance in alkaline medium. High specific energy density and power density could be delivered at the same time for the symmetric EC. The SPD of approximately 1,770 W/kg and SED of approximately 15 Wh/kg were obtained at a current density of 3 A/g. And the SED increased to approximately 21 Wh/kg when the SPD decreased to approximately 850 W/kg. The symmetric EC also demonstrated a cycling performance with an attenuation of SC of approximately 14.8% over 1,000 cycle number. Furthermore, aqueous symmetric ECs based on $Ru_xM_{1-x}O_y{\cdot}nH_2O$ (M = Co, Ni, Ti, Cr, In, V, etc.) oxides operating in alkaline system are expected to own the same good electrochemical performance as that of the EC based on $Ru_{0.7}Sn_{0.3}O_2{\cdot}nH_2O$ electrode. Herein, a new path is now open for future development of aqueous symmetric ECs.

Acknowledgements This work was supported by National Basic Research Program of China (973 Program; No. 2007CB209703), National Natural Science Foundation of China (No. 20403014, No. 20633040), and Natural Science Foundation of Jiangsu Province (BK2006196).

References

1. Conway BE (1991) J Electrochem Soc 138:1539
2. Wang YG, Zhang XG (2004) Electrochim Acta 49:1957
3. Wang YG, Wang ZD, Xia YY (2005) J Power Sources 50:5641
4. Cottineau T, Toupin M, Delahaye T, Brousse T, Bélanger D (2006) Appl Phys A82:599
5. Ganesh V, Pitchumani S, Lakshminarayanan V (2006) J Power Sources 158:1523
6. Homenko VK, Raymundo-Pinero E, Frackowiak E, Béguin F (2006) Appl Phys A82:567
7. Frackowiak E, Béguin F (2001) Carbon 39:937
8. Zheng JP, Jow TR (1997) J Electrochem Soc 144:2417
9. Balducci A, Dugas R, Taberna PL, Simon P, Plée D, Mastragostino M, Passerini S (2007) J Power Sources 165:922
10. Chang KH, Hu CC (2005) Electrochim Acta 50:2573
11. Hu CC, Wang CC, Chang KH (2007) Electrochim Acta 52:2691
12. Hu CC, Chang KH, Wang CC (2007) Electrochim Acta 52:4411
13. Hu CC, Chuang PY, Wu YT (2005) J Electrochem Soc 152:A370
14. Soudan P, Gaudet J, Guay D, Bélanger D, Schulz R (2002) Chem Mater 14:1210
15. Yokoshima K, Shibutani T, Hirota M, Sugimoto W, Murakami Y, Takasu Y (2006) J Power Sources 160:1480
16. Li J, Wang XY, Huang QH, Dai CL, Gamboa S, Sebastian PJ (2007) J Appl Electrochem 37(10):1129 DOI 10.1007/s10800-007-9372-7
17. Liu Y, Zhao WW, Zhang XG (2007) Electrochim Acta DOI 10.1016/j.electacta.2007.11.022
18. Gao B, Zhang XG, Yuan CZ, Li J, Yu L (2006) Electrochim Acta 52:1028
19. Bonnefoi L, Simon P, Fauvarque JF, Sarrazin C, Sarrau JF, Dugast A (1999) J Power Sources 80:149
20. Bonnefoi L, Simon P, Fauvarque JF, Sarrazin C, Dugast A (1999) J Power Sources 79:37
21. Lufrano F, Staiti P, Minutoli M (2004) J Electrochem Soc 151:A64
22. Jiang JH, Kucernak A (2002) Electrochim Acta 47:2381
23. Liang YY, Li HL, Zhang XG (2008) Mater Sci Eng A 473:317
24. Wang YG, Cheng L, Xia YY (2006) J Power Sources 153:191
25. Yuan CZ, Zhang XG, Wu QF, Gao B (2006) Solid State Ionics 177:1237
26. Wang YG, Wang ZD, Xia YY (2005) Electrochim Acta 50:5641
27. Michael MS, Prabaharan SR (2004) J Power Sources 136:250
28. Yuan CZ, Gao B, Zhang XG (2007) J Power Sources 173:606
29. Trasatti S (1991) Electrochim Acta 36:225
30. Hu CC, Lee CH, Wen TC (1996) J Appl Electrochem 26:72
31. Wen TC, Hu CC (1992) J Electrochem Soc 139:2158
32. Onuchukwu AI, Trasatti S (1991) J Appl Electrochem 21:858
33. Comninellis CH, Verchsi GP (1991) J Appl Electrochem 21:136
34. Lin SM, Wen TC (1993) J Electrochem Soc 140:2265
35. Abbizzani C, Mastragostino M, Meneghello L (1995) Electrochim Acta 40:2223
36. Feng T, Zhao YQ, Zhang GQ, Li HL (2007) Eletrochem Commun 9:1282
37. Muthulakshmi B, Kalpana D, Pitchumani S Renganathan NG (2006) J Power Sources 158:1533